# Symmetric mass-division process in nuclei with mass numbers around ACN=100



| | |
|---|---|
| 著者 | 大槻　勤 |
| journal or publication title | Physical review. C |
| volume | 47 |
| number | 4 |
| page range | 1586-1594 |
| year | 1993 |
| URL | http://hdl.handle.net/10097/35723 |

doi: 10.1103/PhysRevC.47.1586

# Symmetric mass-division process in nuclei with mass numbers around $A_{\mathrm{CN}}=100$

Y. Nagame, H. Ikezoe, and T. Ohtsuki*
*Japan Atomic Energy Research Institute, Tokai-mura, Ibaraki 319-11, Japan*
(Received 8 September 1992)

Mass, angular, and total-kinetic-energy distributions for symmetric mass division products of the compound nucleus (CN) $^{105}$Ag formed in the $^{37}$Cl+$^{68}$Zn and $^{16}$O+$^{89}$Y reactions have been measured with a time-of-flight telescope. The characteristics of the products are consistent with those of the fission products obtained in the heavier mass systems. A remarkable angular momentum effect on the width of the mass and total kinetic energy distributions is observed. The features of symmetric mass division products in nuclei with mass numbers around $A_{\mathrm{CN}}=100$ are summarized and systematically examined in terms of corresponding angular momentum.

PACS number(s): 25.70.Jj, 25.85.Ge

## I. INTRODUCTION

The symmetric mass-division process of lighter compound nuclei (CN) with mass numbers around $A_{\mathrm{CN}}=100$ is little understood because it is difficult to identify the signatures of the process. In this mass region, it is of considerable interest to investigate the Businaro-Gallone (BG) limit based on the liquid-drop model [1]. For nuclei with fissility parameter $x$ smaller than the BG limit $x_{\mathrm{BG}}=0.396$ and with a zero angular momentum, the saddle-point energy shows a maximum at symmetry in the mass-asymmetry coordinate; a deforming nucleus becomes unstable toward asymmetric deformation on its way from a saddle to a scission point. This saddle-point energy is called as the conditional barrier and the ridge-point potential-energy surface [2–4]. As angular momentum $l$ brought into a compound nucleus increases, the conditional barrier decreases at mass symmetry and two BG mountains appear at the mass-asymmetry region. The angular momentum effect lowers the BG limit. This feature of the $l$-dependent potential-energy surfaces $B(l)$ is illustrated in Fig. 1 as a function of the mass asymmetry for the compound nucleus $^{105}$Ag. The calculation of $B(l)$ is based on the liquid-drop model and will be discussed in Sec. III. The $l$-dependent yield $Y(l)$ in the compound-nucleus decay is expressed as

$$Y(l)\propto\exp[-B(l)/T_S(l)]\ , \tag{1}$$

where $T_S(l)$ is the saddle-point temperature as defined in Sec. III. At high angular momentum, a symmetric mass division is expected even in light-mass systems with $x$ smaller than $x_{\mathrm{BG}}$.

Several experimental efforts have been made to confirm the symmetric mass-division process and to study features of the conditional barriers in nuclei lighter than $A_{\mathrm{CN}}\sim 100$. A binary symmetric mass division in these light composite nuclei formed by heavy-ion reactions has been verified with the coincidence method [5–15]. Yields of fissionlike products were reported by several authors [16–32], although certain ambiguities as to the nature of the products still remain. An experimental confirmation of the BG transition has also been extensively studied [33–43]. Few approaches, however, have been made to study the $l$ dependence of mass and kinetic-energy distributions in this mass region.

The aim of the present work is to elucidate the presence of the symmetric mass-division process in light nuclei with mass numbers around $A_{\mathrm{CN}}=100$ and to study the role of angular momentum. In this paper we present the measured mass, angular, and total-kinetic-energy distributions of the products for the symmetric mass division of the $^{105}$Ag formed in the $^{37}$Cl+$^{68}$Zn and the $^{16}$O+$^{89}$Y reactions. Since the two reaction systems produce the same compound nucleus $^{105}$Ag, one expects to see the dependence of angular momentum and excitation energy on mass and kinetic-energy distributions of the symmetric mass-division products. Systematic features of mass and kinetic-energy distributions for the symmetric mass-division products in this mass region are examined in terms of the corresponding angular momentum. Part of this work has been published elsewhere [32].

## II. EXPERIMENTAL PROCEDURES

Beams of $^{37}$Cl with energies of 160 and 177 MeV and $^{16}$O with 140 MeV from the JAERI (Japan Atomic Energy Research Institute) tandem accelerator were used to bombard self-supporting targets of $^{68}$Zn (755 $\mu$g/cm$^2$ thick and 99.34% enrichment) and $^{89}$Y (433 $\mu$g/cm$^2$ thick), respectively.

The mass distribution of the products was measured with a time-of-flight (TOF) telescope. The start detector was composed of a carbon foil (30 $\mu$g/cm$^2$ thick) microchannel plate [44]. The stop and energy signals were delivered with a 250-$\mu$g/cm$^2$-thick Si surface barrier detector located at about 65 cm from the start detector.

*Permanent address: Laboratory of Nuclear Science, Tohoku University, Taihaku-ku, Sendai 982, Japan.

 

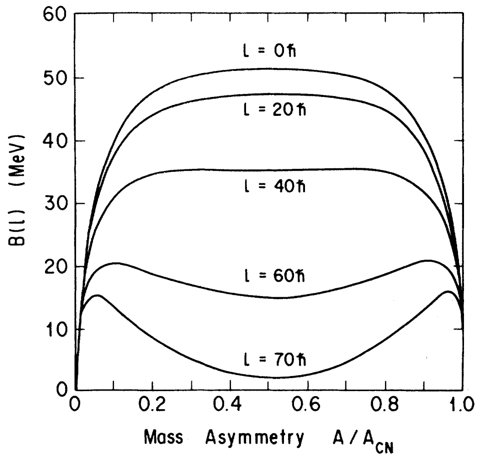


FIG. 1. Potential-energy surfaces at the saddle point for different angular momenta on the decay of the compound nucleus $^{105}$Ag as a function of the mass asymmetry $A/A_{CN}$, where $A_{CN}$ indicates the compound-nucleus mass number.

A fragment mass $A$ was determined as $A \propto Et^2$ from the flight time $t$ and the kinetic energy $E$ corrected for pulse-height defect in a Si surface barrier detector. The pulse-height defect was estimated using the systematics of Moulton *et al.* [45].

The energy calibration was performed by using the elastically scattered projectiles from a 100-$\mu$g/cm$^2$-thick $^{197}$Au target at high energies and $\alpha$ particles from an $^{241}$Am source at low energy. The time calibration was carried out by a high-precision time calibrator. An overall time resolution of approximately 280 ps was achieved.

The data taken at various angles were normalized to the elastic scattering events at small angles.

## III. RESULTS AND DISCUSSION

### A. Experimental results and discussion

Measured mass distributions in the center-of-mass (c.m.) system are displayed in Figs. 2–4. The transformation of the mass distribution from the laboratory system to the c.m. system was carried out event by event using the method described in [46]. To obtain the primary mass fragments, corrections for neutron evaporation from fragments were made by assuming that the compound-nucleus excitation energy is shared between fragments in proportion to their masses [44,46] and that deexcitation of fragments occurs mainly via neutron evaporation and $\gamma$-ray emission [23]. Energies carried away via neutron and $\gamma$-ray emissions were assumed to be $2T$ and 10 MeV, respectively. The nuclear temperature $T$ was given by $T=\sqrt{E_{ex}/a}$, with $a = A/8.5$. The excitation energy $E_{ex}$ of a product mass $A$ is expressed as

$$E_{ex}=(E^*_{CN}+Q-E_{TKE})A/A_{CN} , \quad (2)$$

where $E^*_{CN}$ and $Q$ are the excitation energy of the compound nucleus and the $Q$ value for mass division. The total kinetic energy (TKE) of the fragments was obtained by assuming two-body kinematics.

As shown in Figs. 2 and 3, the products corresponding to the nucleon transfer reactions are located around the projectile mass $A_P$ of $^{37}$Cl and the target mass $A_T$ of $^{68}$Zn. These products strongly depend on the angle; the projectilelike products appear at more forward angles, while the bump of the targetlike recoil products is observed at backward angles. At forward angles $\theta_{lab}=15°$ and 20°, one can see the products of symmetric mass division apart from the nucleon transfer reaction products. Since we focus on the symmetric mass-division process, the mass distributions taken at these forward angles will be used in the following discussion. In the $^{16}$O + $^{89}$Y system shown in Fig. 4, the peak of the symmetric mass division is clearly seen, while the components of projec-

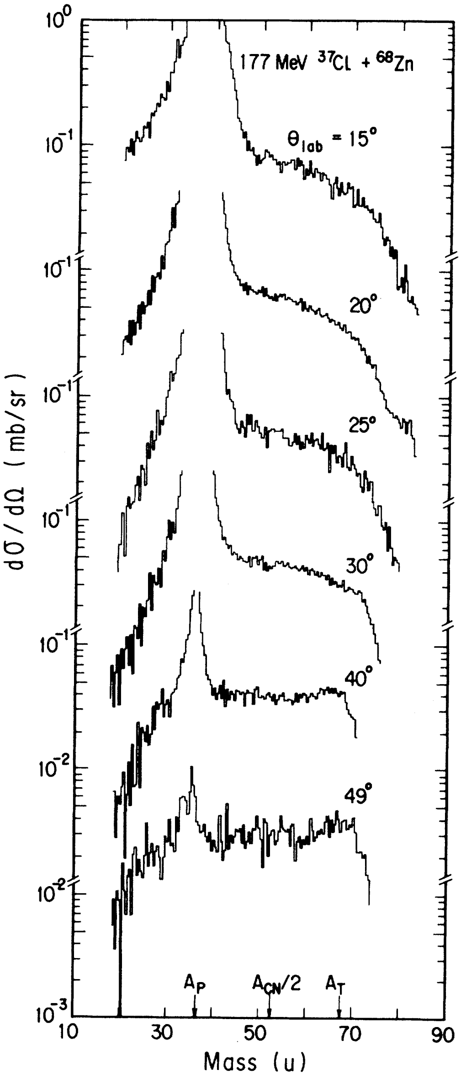


FIG. 2. Fragment mass distributions for the reaction 177 MeV $^{37}$Cl + $^{68}$Zn. The symbols $A_P$ and $A_T$ correspond to the mass numbers of the projectile and target nucleus.

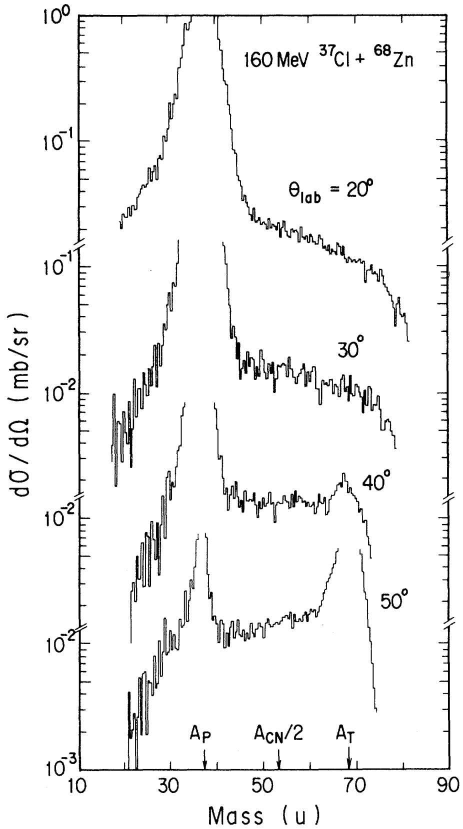


FIG. 3. Same as Fig. 2 for the reaction 160 MeV $^{37}$Cl + $^{68}$Zn.

tilelike and targetlike products appear in the mass regions of $A \leq 40$ and $A \geq 65$, respectively.

Figure 5 shows the mass distributions for the symmetric mass-division products. To avoid the contaminants from projectilelike products, the mass distributions are cut off below $A \sim 50$ in the $^{37}$Cl + $^{68}$Zn system. As shown in Figs. 5(a) and 5(b), no clear scattering angle dependence is observed in the symmetric mass region and there is no evidence for a peak around $A_T$. The dashed lines are a least-squares fit to the data by a Gaussian function having the center at $\frac{1}{2}A_{CN}$. In the $^{16}$O + $^{89}$Y system, a Gaussian fit was performed to the data at $\theta_{lab}=35°$.

In Fig. 6 are shown the angular distributions for the symmetric mass-division products. The differential cross sections for the $^{16}$O + $^{89}$Y system are obtained from the integration of the symmetric mass distributions, while those in the $^{37}$Cl + $^{68}$Zn are from the mass region $50 \leq A \leq 55$ to eliminate the contaminants from the nucleon transfer products. The angular distributions of the symmetric mass-division products are essentially flat in $d\sigma/d\theta_{c.m.}$, as expected for the fission products of the compound nucleus or the decay products of a long-lived

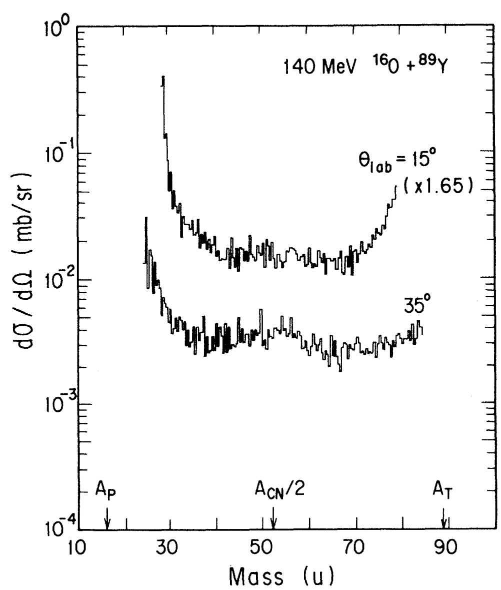


FIG. 4. Same as Fig. 2 for the reaction 140 MeV $^{16}$O + $^{89}$Y.

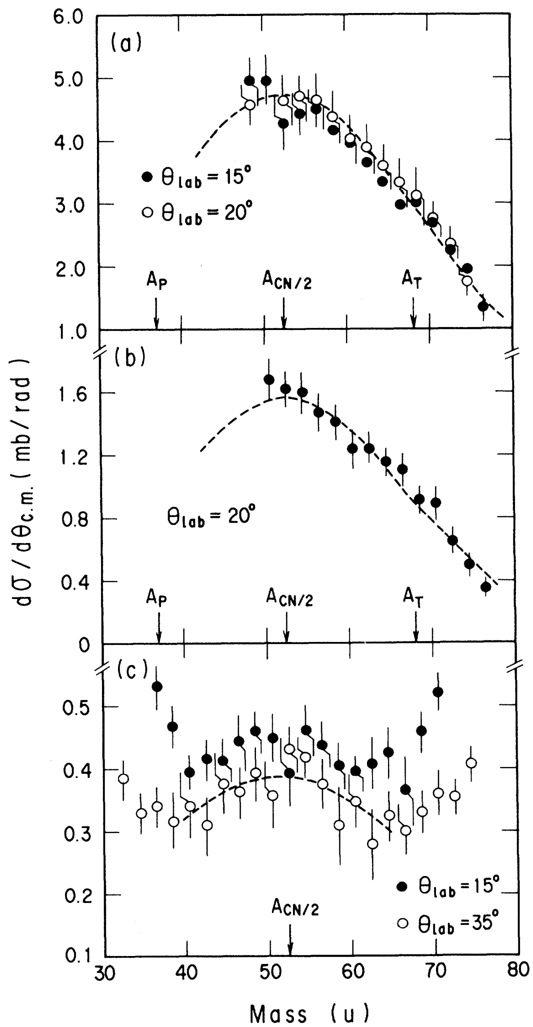


FIG. 5. Mass distributions for the symmetric mass-division products for (a) 177 MeV $^{37}$Cl + $^{68}$Zn, (b) 160 MeV $^{37}$Cl + $^{68}$Zn, and (c) 140 MeV $^{16}$O + $^{89}$Y. The dashed lines are a least-squares fit by a Gaussian function.

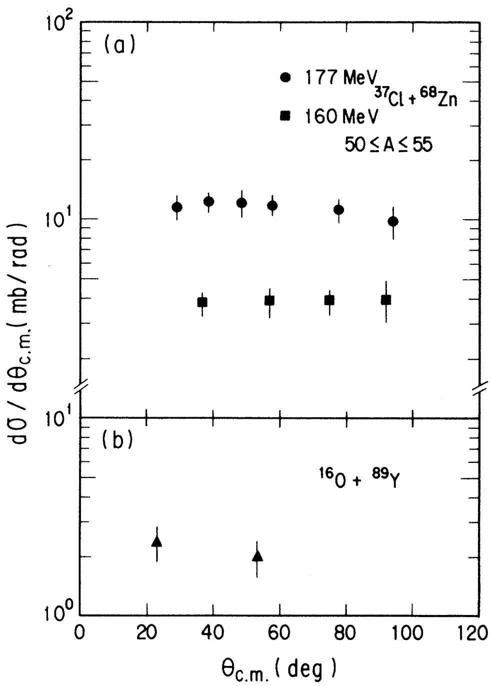


FIG. 6. Center-of-mass angular distributions for the symmetric mass-division products. The differential cross sections for the $^{16}O + ^{89}Y$ system are the integrated values of the mass distributions, while those in the $^{37}Cl + ^{68}Zn$ are from the mass region of $50 \leq A \leq 55$.

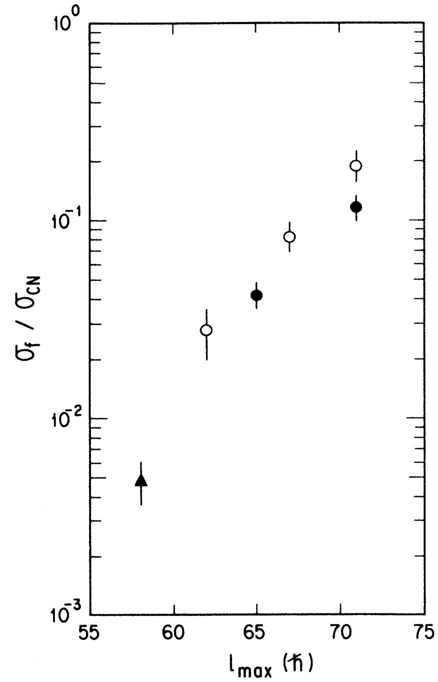


FIG. 7. Ratio of the cross sections $\sigma_f$ for the symmetric mass-division process to the fusion cross sections $\sigma_{CN}$ as a function of the corresponding $l_{max}$ for the $^{37}Cl + ^{68}Zn$ (●) and the $^{16}O + ^{89}Y$ (▲) systems. The open symbols are taken from Ref. [14].

dinuclear system, indicating that the composite system has reached an equilibrium state in all the degrees of freedom prior to scission.

In Fig. 7 ratios of the cross sections $\sigma_f$ for the symmetric mass-division products to the fusion cross sections $\sigma_{CN}$ by the Bass model [47] are plotted as a function of the corresponding maximum angular momentum $l_{max}$. The angle-integrated cross sections $\sigma_f$ were obtained by assuming an isotropic form of $d\sigma/d\theta_{c.m.}$ angular distributions. It is clearly seen that the ratio exponentially increases with $l_{max}$ in the $l$ region studied, indicating that the probability of the symmetric mass-division process strongly depends on $l_{max}$.

The experimental cross sections are compared with prediction of a statistical compound-nucleus model. The statistical-model analysis of fission decay has been carried out by means of the computer code PACE2 [48]. The angular momentum dependence of the fission barrier and the yrast line up to the maximum angular momentum [48] were taken from the rotating finite-range model (RFRM) of Sierk [49]. Fits to the data were made using the default parameters; the scaling factor $k$ of the fission barrier that determines the slope of the calculated excitation function was 1.0, and the ratio of the level-density parameter for fission to that of particle emission $a_f/a_v$ was set to unity. The fusion cross sections were obtained by using the Bass potential [47]. The comparisons between the experimental values and the calculations are shown in Fig. 8 as a function of the compound-nucleus

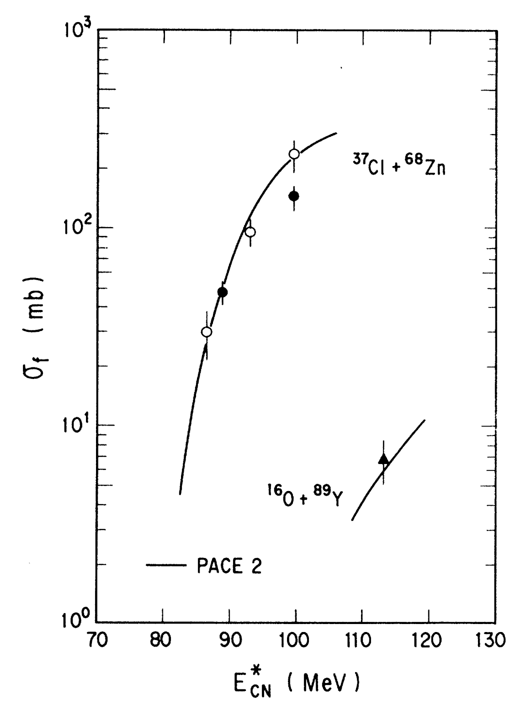


FIG. 8. Comparison of the experimental cross sections for the symmetric mass-division process and the calculated fission cross sections. The solid lines represent the calculated values with the PACE2 code [48]. The open symbols are taken from Ref. [14].

excitation energy. The figure shows that the experimental cross sections are well reproduced by the calculation, indicating that the observed symmetric mass-division processes are consistent with the statistical fission decay.

In Fig. 9 the mean total kinetic energy $\langle E_{TKE} \rangle$ and the variance $\sigma_{TKE}$ of TKE distributions are plotted as a function of the c.m. scattering angle. The variances $\sigma_{TKE}$ are obtained by assuming a Gaussian function for TKE distributions. The width of the fission-fragment TKE distribution is expected to broaden with the nuclear temperature $T_S$ at the saddle point [50]. The experimental variances are reduced to the values at $T_S=1.6$ MeV and $l=l_{max}$ [32],

$$\sigma_{TKE}=\sigma_{TKE}^{expt}/\sqrt{T_S(l_{max})/1.6} \ , \tag{3}$$

where $l_{max}$ is the maximum angular momentum for fusion taken from the prediction of Bass [47]. Since the symmetric mass-division process is prominent at a higher-$l$ region as discussed above, $l_{max}$ will be used in the following discussion on $l$ effects. The $l$-dependent saddle-point temperature $T_S(l)$ is given by [51,14]

$$\frac{1}{T_S(l)}=\left[\frac{a}{E_{CN}^*(l)-B_S(l)}\right]^{1/2} - \left[\frac{2}{E_{CN}^*(l)-B_S(l)}\right] . \tag{4}$$

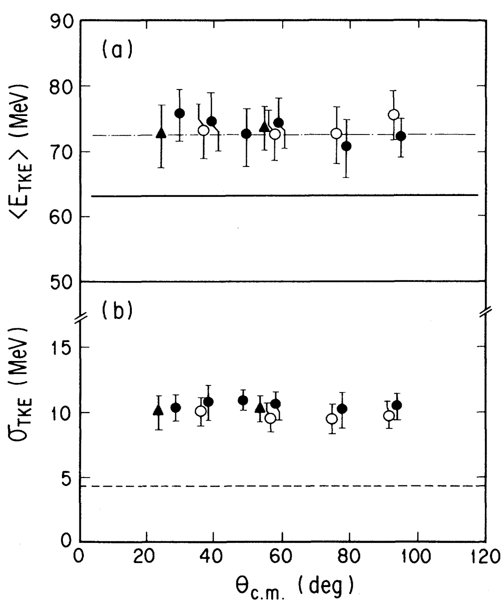


FIG. 9. Mean total kinetic energy $\langle E_{TKE} \rangle$ and variance $\sigma_{TKE}$ of the TKE distributions as a function of the c.m. scattering angle for the 160 MeV $^{37}Cl$ + $^{68}Zn$ (○), 177 MeV $^{37}Cl$ + $^{68}Zn$ (●), and 140 MeV $^{16}O$ + $^{89}Y$ (▲). The solid and dot-dashed lines in (a) show the values expected from the empirical formulas of Viola, Kwiatkowski, and Walker [54] and [55], respectively. The dashed line in (b) indicates the predicted value of $\sigma_{TKE}$ by the liquid-drop model of Nix [50] at the saddle-point temperature 1.6 MeV (see text).

The level-density parameter $a$ is fixed as $a=A/8.5$ MeV$^{-1}$ [51]. The $E_{CN}^*(l)$ is $l$-dependent compound-nucleus excitation energy [14]:

$$E_{CN}^*(l)=E_{c.m.}+Q_{gg}-E_{rot}^{CN}(l) \ , \tag{5}$$

with $Q_{gg}$ representing the ground-state reaction $Q$ value, $E_{c.m.}$ the bombarding energy in the c.m. system, and $E_{rot}^{CN}$ the rotational ground-state energy of a compound nucleus. The $l$-dependent potential energy $B(l)$ is [14]

$$B(l)=(U_1+U_2-U_{CN})+U_C+U_N + [E_{rot}^{SP}(l)-E_{rot}^{CN}(l)] \ , \tag{6}$$

where $U_1$, $U_2$, and $U_{CN}$ are the liquid-drop masses [52] of fragments 1,2 and a compound nucleus. The Coulomb repulsion energy is denoted by $U_C$, and two touching spheres are assumed as the saddle-point configuration. The nuclear attractive force $U_N$ of two fragments was obtained from the proximity potential [53]. The rotational energy of the saddle-point configuration, $E_{rot}^{SP}$, was calculated by assuming the sticking limit.

As shown in Fig. 9, $\langle E_{TKE} \rangle$ and $\sigma_{TKE}$ are practically independent of the scattering angle. The dot-dashed and solid lines in Fig 9(a) show the expected values from the empirical formulas of Viola, Kwiatkowski, and Walker [54,55]. The systematics in the 1966 version reproduces well the present $\langle E_{TKE} \rangle$ values. These results show that the reactions considered are characterized by a fully kinetic-energy relaxation of the initial relative motion. No significant dependence on the corresponding angular momentum and excitation energy is observed in $\langle E_{TKE} \rangle$ and $\sigma_{TKE}$ in the studied $l$ and $E_{CN}^*$ regions.

The dashed line in Fig. 9(b) indicates the value predicted from the liquid-drop model of Nix [50] in which the nuclear temperature at the saddle point is fixed to

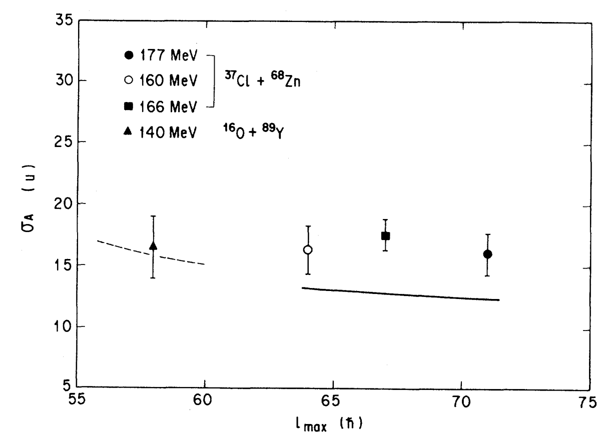


FIG. 10. Variances of the mass distributions for the symmetric mass-division process as a function of $l_{max}$. The internal excitation energy of the composite system is normalized to an excitation energy corresponding to $T_S(l_{max})=1.6$ MeV. The value for the 166 MeV $^{37}Cl$ + $^{68}Zn$ reaction (open circle) is taken from Ref. [14]. The solid and dashed lines are the variances predicted from the static-model calculation based on the potential-energy surfaces in Fig. 1 for the $^{37}Cl$ + $^{68}Zn$ and $^{16}O$ + $^{89}Y$, respectively.

$T_S = 1.6$ MeV. The experimental widths are considerably larger than the calculated widths. Similar results were reported in heavy-ion-induced fission of heavier-mass systems [56,57].

The measured variances $\sigma_A^{\text{expt}}$ from the dashed lines in Fig. 5 at a nuclear temperature $T_S(l)$ are normalized to values corresponding to $T_S(l_{\max}) = 1.6$ MeV as

$$\sigma_A = \sigma_A^{\text{expt}} \sqrt{T_S(l_{\max})/1.6} \ . \quad (7)$$

In Fig. 10 the corrected $\sigma_A$ values are plotted as a function of $l_{\max}$. It is found that the $\sigma_A$ values are independent of $l_{\max}$ in the studied $l$ region. Assuming that the shape of the mass distribution depends only on that of the static potential-energy surfaces shown in Fig. 1, the width of the corresponding mass distribution is expected to become narrower as angular momentum increases [58]. The solid and dashed lines are the calculated values expected from the static potential-energy surfaces for the systems $^{37}$Cl + $^{68}$Zn and $^{16}$O + $^{89}$Y, respectively. The observed constancy of $\sigma_A$ as a function of $l$ is inconsistent with the prediction: the deviation of the experimental variances from the calculations increases with $l_{\max}$. The same trend that the $\sigma_A$ values are nearly independent of $l_{\max}$ was reported by Glagora, Back, and Betts [57] and Itkis *et al.* [59] in the mass region around $A_{\text{CN}} = 180-200$.

According to the consideration by Faber [60], the stiffness of the potential energy associated with the mass-asymmetry degree of freedom at a saddle point is expect-

TABLE I. List of the reactions studied in the present work with relevant parameters.

| Reaction | Compound nucleus | $x^{a}$ | $E_{\text{lab}}$ (MeV) | $E_{\text{CN}}^{*\,b}$ (MeV) | $l_{\max}$ $^{c}$ ($\hbar$) | $y^{d}$ | Reference |
|---|---|---|---|---|---|---|---|
| $^{6}$Li + $^{40}$Ca | $^{46}$V | 0.226 | 153 | 149 | 28 | 0.199 | [9] |
| $^{9}$Be + $^{40}$Ca | $^{49}$Cr | 0.231 | 141 | 137 | 34 | 0.253 | [9] |
| $^{12}$C + $^{40}$Ca | $^{52}$Fe | 0.255 | 186 | 156 | 45 | 0.386 | [9] |
| $^{63}$Cu + $^{12}$C | $^{75}$Br | 0.324 | 794 | 132 | 39 | 0.124 | [41] |
| $^{14}$N + $^{58,60}$Ni | $^{(73)}$Br | 0.331 | 126 | ~107 | 45 | 0.176 | [5] |
| $^{32}$S + $^{50}$Ti | $^{82}$Sr | 0.349 | 140 | 84 | 54 | 0.194 | [6] |
| $^{14}$N + $^{\text{nat}}$Se | $^{(93)}$Nb | 0.364 | 126 | ~121 | 50 | 0.126 | [5] |
| $^{63}$Cu + $^{27}$Al | $^{90}$Mo | 0.386 | 794 | 234 | 71 | 0.269 | [41] |
| $^{40}$Ca + $^{40}$Ca | $^{80}$Zr | 0.393 | 197 | 85.6 | 56 | 0.219 | [15] |
| $^{93}$Nb + $^{9}$Be | $^{102}$Rh | 0.400 | 782 | 78 | 34 | 0.047 | [38] |
| $^{12}$C + $^{89}$Y | $^{101}$Rh | 0.403 | 197 | 173 | 62 | 0.159 | [16] |
| $^{35}$Cl + $^{62}$Ni | $^{97}$Rh | 0.407 | 170 | 95.2 | 66 | 0.196 | [20] |
| $^{37}$Cl + $^{68}$Zn | $^{105}$Ag | 0.422 | 156 | 86.3 | 62 | 0.145 | [14] |
| | | | 160 | 88.9 | 65 | 0.159 | present work |
| | | | 166 | 92.8 | 67 | 0.169 | [14] |
| | | | 177 | 99.9 | 71 | 0.190 | [14], present work |
| $^{16}$O + $^{89}$Y | $^{105}$Ag | 0.422 | 140 | 113.3 | 58 | 0.127 | present work |
| $^{93}$Nb + $^{12}$C | $^{105}$Ag | 0.422 | 1060 | 121 | 51 | 0.098 | [38] |
| | | | 1367 | 156 | 59 | 0.131 | [38] |
| | | | 1674 | 191 | 66 | 0.164 | [38] |
| $^{12}$C + $^{98}$Mo | $^{110}$Cd | 0.424 | 197 | 178 | 64 | 0.140 | [16,17] |
| $p$ + $^{\text{nat}}$Ag | $^{(109)}$Cd | 0.426 | 600 | ~240 | 26 | 0.024 | [18,19] |
| $^{84}$Kr + $^{24}$Mg | $^{108}$Cd | 0.429 | 487 | 101 | 62 | 0.136 | [24] |
| $^{32}$S + $^{76}$Ge | $^{108}$Cd | 0.429 | 158 | 101 | 67 | 0.159 | [23] |
| | | | 178 | 115 | 73 | 0.189 | [23] |
| | | | 198 | 129 | 79 | 0.221 | [23] |
| | | | 218 | 143 | 85 | 0.256 | [23] |
| | | | 225 | 148 | 87 | 0.268 | [23] |
| $^{84}$Kr + $^{27}$Al | $^{111}$In | 0.436 | 496 | 108 | 64 | 0.137 | [25] |
| $^{14}$N + $^{\text{nat}}$Mo | $^{(110)}$In | 0.438 | 126 | ~110 | 52 | 0.092 | [5] |
| $^{45}$Sc + $^{65}$Cu | $^{110}$Sn | 0.453 | 200 | 94 | 70 | 0.165 | [12] |
| $^{20}$Ne + $^{100}$Mo | $^{120}$Te | 0.457 | 146 | 118.2 | 64 | 0.115 | [29] |
| $^{12}$C + $^{\text{nat}}$Ag | $^{(120)}$I | 0.472 | 107 | ~93 | 46 | 0.059 | [16] |
| | | | 197 | ~174 | 65 | 0.117 | [16] |
| $^{20}$Ne + $^{92}$Mo | $^{112}$Te | 0.479 | 146 | 103.7 | 61 | 0.120 | [29] |
| $^{14}$N + $^{\text{nat}}$Ag | $^{(122)}$Xe | 0.481 | 126 | ~112 | 54 | 0.078 | [5] |
| $^{12}$C + $^{116}$Sn | $^{128}$Ba | 0.495 | 197 | 172 | 67 | 0.108 | [16] |

[a]Fissility parameter $x = (Z^2/A)/[50.883(1-1.7826I^2)]$, where $I = (N-Z)/A$. $N$, $Z$, and $A$ are the neutron, proton, and mass numbers of the compound nucleus [61].

[b]Compound-nucleus excitation energy.

[c]Maximum angular momentum for fusion predicted by Bass [47].

[d]$y = [1.9249/(1-1.7826I^2)] l_{\max}^2 / A^{7/3}$ [61].

ed to decrease with $l$. The mass distribution would become wider than predicted by the static potential-energy surface with $l$. The observed trend of $\sigma_A$ in Fig. 9 would be qualitatively explained by this model.

Although the effect of $l$ on $\sigma_{\mathrm{TKE}}$ and $\sigma_A$ has not yet been fully accounted for in a quantitative manner, the observed broad width would be interpreted as a contribution of some dynamical effects including $l$ to the symmetric mass-division process.

### B. Systematics of symmetric mass-division process in nuclei with mass numbers around $A_{\mathrm{CN}}=100$

The systematic features of symmetric mass-division products on cross sections, TKE, and mass distributions are discussed over a wide range of $l_{\max}$. The reaction systems studied in this work are listed in Table I together with the relevant parameters.

Cross sections $\sigma_f$ for the symmetric mass-division process are summarized in Fig. 11 as a function of corresponding $l_{\max}$. The data are taken from Refs. [14, 19, 20, 23, 25, 29]. Except for the $p+{}^{\mathrm{nat}}\mathrm{Ag}$ system [19], the $\sigma_f$ values increase smoothly with $l_{\max}$ and it seems to indicate the threshold of $l_{\max}\sim 55\hbar$ for the symmetric mass division. According to the RFRM [49], the corresponding fission barrier $B_f$ at $l_{\max}\sim 55\hbar$ is about 10 MeV around the $A_{\mathrm{CN}}=100$ region. It is nearly equal to the neutron binding energy of a compound nucleus. This shows that the neutron evaporation process is dominant at $l_{\max}<55\hbar$, while the fission process competes with the evaporation beyond $l_{\max}\sim 55\hbar$.

The $\langle E_{\mathrm{TKE}}\rangle$ values observed in Refs. [5, 6, 9, 12, 14–16, 19, 20, 38, 41] are compared with the empirical formulas predicted by Viola, Kwiatkowski, and Walker [54,55] in Fig. 12. The experimental $\langle E_{\mathrm{TKE}}\rangle$ values are well reproduced with the systematics in the 1966 version except for the data of Refs. [16,19]. Reevaluation of the formula by using the new data would be needed in the region around $Z^2/A^{1/3}=400-600$.

In Fig. 13 the corrected $\sigma_{\mathrm{TKE}}$ values corresponding to $T_S(l_{\max})=1.6$ MeV are plotted as a function of $l_{\max}$ for the systems in Refs. [5, 6, 14, 19, 41]. As shown in Fig. 13, although the data are scattered, the $\sigma_{\mathrm{TKE}}$ tends to increase with increasing $l_{\max}$ in the indicated $l_{\max}$ region.

The $\sigma_A$ values corrected by Eq. (7) taken from Refs. [5, 12, 14, 17, 19, 20, 23, 24, 29] are shown in Fig. 14 as a function of $l_{\max}$. It can be seen that the mass distributions become wider with increasing $l_{\max}$ over a wide range of $l_{\max}$. As discussed in the previous section, the stiffness of the potential energy associated with the mass-asymmetry degree of freedom at a saddle point is expected to decrease as $l$ increases.

A dynamical model calculation associated with $l$ is

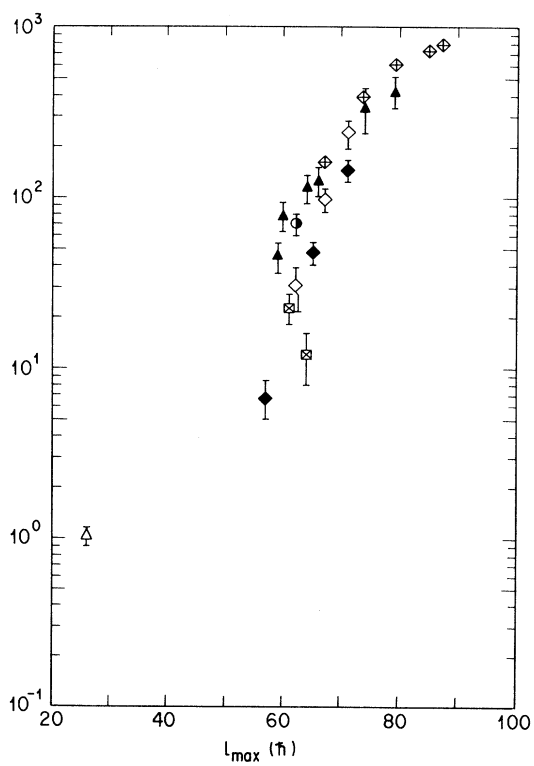


FIG. 11. Cross sections for the symmetric mass-division products as a function of corresponding $l_{\max}$. The data are taken from Refs. [14] (◇), [19] (△), [20] (▲), [23] (⊕), [25] (◑), [29] (□), and the present work (◆).

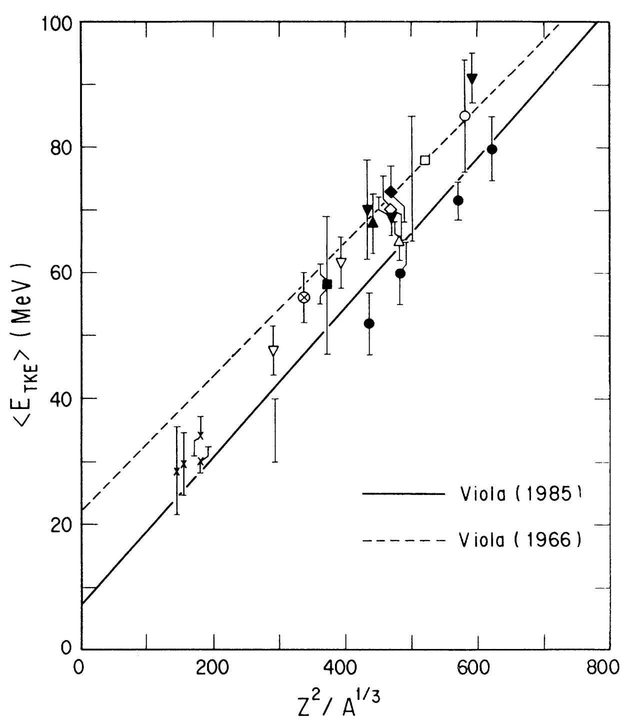


FIG. 12. Mean total kinetic energies for symmetric mass-division products taken from Refs. [5] (○ and I), [6] (⊗), [9] (×), [12] (□), [14] (◇), [15] (■), [16] (●), [19] (△), [20] (▲), [38] (▼), [41] (▽), and the present work (◆) as a function of the Coulomb parameter $Z^2/A^{1/3}$ of fissioning nuclei. Empirical curves for fission kinetic-energy release are shown by solid [54] and dashed [55] lines.

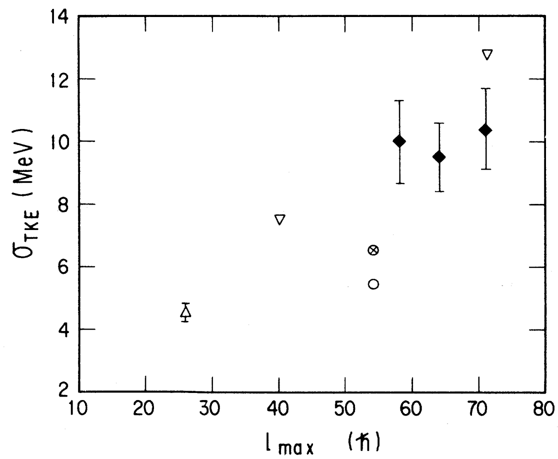


FIG. 13. Variances of TKE distributions for the symmetric mass-division products as a function of $l_{max}$. The internal excitation energy of the composite system is normalized to an excitation energy corresponding to $T_S(l_{max})=1.6$ MeV. The experimental $\sigma_{TKE}$ are taken from Refs. [5] (○), [6] (⊗), [14] (◇), [19] (△), [41] (▽), and the present work (◆).

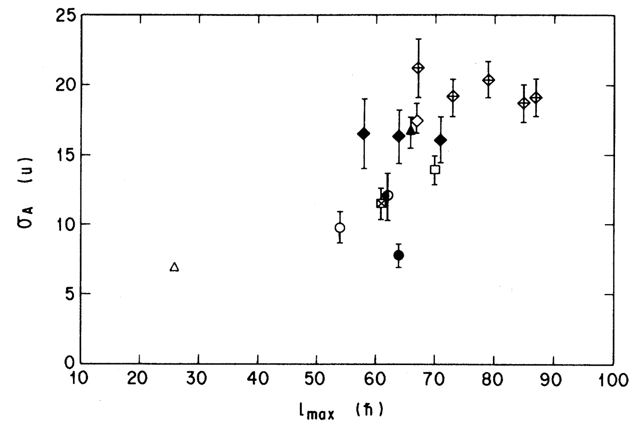


FIG. 14. Variances of the mass distributions for the symmetric mass-division products as a function of $l_{max}$. The internal excitation energy of the composite system is normalized to an excitation energy corresponding to $T_S(l_{max})=1.6$ MeV. The data are taken from Refs. [5] (○), [12] (□), [14] (◇), [17] (●), [19] (△), [20] (▲), [23] (⊕), [24] (◐), [29] (⊠), and the present work (◆).

needed to explain the widths of the total-kinetic-energy and mass distributions. Much more experimental and theoretical work is necessary before we attain a good quantitative understanding of the symmetric mass-division process in light systems.

## IV. CONCLUSION

The observed mass, angular, and total-kinetic-energy distributions of the fully energy-damped symmetric mass-division products of $^{105}$Ag formed in the reactions $^{37}$Cl + $^{68}$Zn and $^{16}$O + $^{89}$Y are consistent with those from the fission products in heavier-mass systems. The cross sections of these products are well reproduced by the statistical-model calculation. These results suggest that the products for the symmetric mass division originate from the symmetric fission of the compound nucleus. A significant angular momentum effect on the mass and total-kinetic-energy distributions and cross sections has been observed. From the systematic interpretation on the characteristics of symmetric mass-division products in a wider range of angular momentum $l$, we confirm a remarkable $l$ effect in the width of mass and TKE distributions and cross sections of symmetric mass-division products in nuclei with mass number around $A_{CN}=100$. The broad widths of the mass and TKE distributions cannot be accounted for the liquid-drop model. This feature should be explained by some dynamical effects including $l$ at a saddle point.

## ACKNOWLEDGMENTS

The authors wish to acknowledge the crew of the JAERI tandem accelerator for the accelerator operation. Thanks are due to the staff of the nuclear chemistry group of JAERI for their support and encouragement during this work.


[1] U. L. Businaro and S. Gallone, Nuovo Cimento **1**, 629 1277 (1955).
[2] L. G. Moretto, Nucl. Phys. **A247**, 211 (1975).
[3] K. T. R. Davies and A. J. Sierk, Phys. Rev. C **31**, 915 (1985).
[4] A. J. Sierk, Phys. Rev. Lett. **55**, 582 (1985).
[5] C. Cabot, C. Ngô, J. Péter, and B. Tamain, Nucl. Phys. **A244**, 134 (1975).
[6] C. K. Gelbke, P. Braun-Munzinger, J. Barrette, B. Zeidman, M. J. Levine, A. Gamp, H. L. Harney, and Th. Walcher, Nucl. Phys. **A269**, 460 (1976).
[7] J. Barrette, P. Braun-Munzinger, C. K. Gelbke, H. E. Wegner, B. Zeidman, A. Gamp, H. L. Harney, and Th. Walcher, Nucl. Phys. **A279**, 125 (1977).
[8] T. C. Awes, R. L. Ferguson, R. Novotny, F. E. Obenshain, F. Plasil, V. Rauch, G. R. Young, and H. Sann, Phys. Rev. Lett. **55**, 1062 (1985).
[9] K. Grotowski, Z. Majka, R. Płaneta, M. Szczodrak, Y. Chan, G. Guarino, L. G. Moretto, D. J. Morrissey, L. G. Sobotka, R. G. Stokstad, I. Tserruya, S. Wald, and G. J. Wozniak, Phys. Rev. C **30**, 1214 (1984).
[10] R. Płaneta, P. Belery, J. Brzychczyk, P. Cohilis, Y. El Masri, Gh. Grégoire, K. Grotowski, Z. Majka, S. Micek, M. Szczodrak, A. Wieloch, and J. Albiński, Phys. Rev. C **34**, 512 (1986).
[11] J. Brzychczyk, K. Grotowski, Z. Majka, S. Micek, R. Płaneta, D. Fabris, K. Hagel, J. B. Natowitz, G. Nebbia, P. Belery, P. Cohilis, Y. El Masri, and Gh. Gregoire, Phys. Lett. B **194**, 473 (1987).
[12] L. G. Sobotka, D. G. Sarantites, Ze Li, E. L. Dines, M. L. Halbert, D. C. Hensley, R. P. Schmitt, Z. Majka, G. Nebbia, H. C. Griffin, and A. J. Sierk, Nucl. Phys. **A471**, 131c (1987).
[13] L. G. Sobotka, D. G. Sarantites, Ze Li, E. L. Dines, M. L. Halbert, D. C. Hensley, J. C. Lisle, R. P. Schmitt, Z. Majka, G. Nebbia, H. C. Griffin, and A. J. Sierk, Phys. Rev. C **36**, 2713 (1987).
[14] Y. Nagame, H. Ikezoe, S. Baba, K. Hata, T. Sekine, S.

Ichikawa, M. Magara, K. Ideno, A. Yokoyama, Y. Hatsukawa, and T. Ohtsuki, Nucl. Phys. **A510**, 518 (1990).
[15] P. M. Evans, A. E. Smith, C. N. Pass, L. Stuttgé, B. B. Back, R. R. Betts, B. K. Dichter, D. J. Henderson, S. J. Sanders, F. Videbaek, and B. D. Wilkins, Nucl. Phys. **A526**, 365 (1991).
[16] M. N. Namboodiri, J. B. Natowitz, E. T. Chulick, K. Das, and L. Webb, Nucl. Phys. **A252**, 163 (1975).
[17] J. B. Natowitz, M. N. Namboodiri, and E. T. Chulick, Phys. Rev. C **13**, 171 (1976).
[18] G. Andersson, M. Areskoug, H.-Å. Gustafsson, G. Hylten, B. Schrøder, and E. Hagebø, Phys. Lett. **71B**, 279 (1977).
[19] G. Andersson, M. Areskoug, H.-Å. Gustafsson, G. Hyltén, B. Schrøder, and E. Hagebø, Z. Phys. A **293**, 241 (1979).
[20] J. Bisplinghoff, P. David, M. Blann, W. Scobel, T. Mayer-Kuckuk, J. Ernst, and A. Mignerey, Phys. Rev. C **17**, 177 (1978).
[21] B. Sikora, W. Scobel, M. Beckerman, J. Bisplinghoff, and M. Blann, Phys. Rev. C **25**, 1446 (1982).
[22] H. Oeschler, P. Wagner, J. P. Coffin, P. Engelstein, and B. Heusch, Phys. Lett. **87B**, 193 (1979).
[23] G. Guillaume, J. P. Coffin, F. Rami, P. Engelstein, B. Heusch, P. Wagner, P. Fintz, J. Barrette, and H. E. Wegner, Phys. Rev. C **26**, 2458 (1982).
[24] B. Heusch, J. P. Coffin, P. Engelstein, G. Guillaume, F. Rami, D. Guerreau, J. Péter, and Z. Zheng, Z. Phys. A **312**, 109 (1983).
[25] B. Heusch, H. Freiesleben, W. F. W. Schneider, B. Kohlmeyer, H. Stege, and F. Pühlhofer, Z. Phys. A **322**, 309 (1985).
[26] I. Iori, M. Gentili, I. Massa, G. Vannini, P. Boccaccio, F. Reffo, L. Vannucci, and R. A. Ricci, Phys. Lett. **132B**, 304 (1983).
[27] S. Agnoli, I. Massa, G. Vannini, P. Boccaccio, F. Reffo, L. Vannucci, I. Iori, and R. A. Ricci, Nucl. Phys. **A464**, 103 (1987).
[28] J. P. Coffin, G. Guillaume, A. Fahli, F. Rami, B. Heusch, P. Wagner, P. Engelstein, P. Fintz, and N. Cindro, Phys. Rev. C **30**, 539 (1984).
[29] Y. Nagame, H. Nakahara, K. Sueki, H. Kudo, I. Kohno, and M. Yanokura, Z. Phys. A **317**, 31 (1984).
[30] S. J. Sanders, R. R. Betts, I. Ahmad, K. T. Lesko, S. Saini, B. D. Wilkins, F. Videbaek, and B. K. Dichter, Phys. Rev. C **34**, 1746 (1986).
[31] P. Boccaccio, L. Vannucci, M. Bettiolo, L. Lavagnini, G. Vannini, I. Massa, R. A. Ricci, I. Iori, G. Guillaume, J. P. Coffin, P. Fintz, and F. Rami, Phys. Rev. C **38**, 2108 (1988).
[32] Y. Nagame, H. Ikezoe, T. Ohtsuki, A. Yokoyama, Y. Hatsukawa, S. Baba, K. Hata, T. Sekine, and K. Ideno, Phys. Lett. B **249**, 13 (1990).
[33] W. Mittig, A. Cunsolo, A. Foti, J. P. Wieleczko, F. Auger, B. Berthier, J. M. Pascaud, J. Quebert, and E. Plagnol, Phys. Lett. **154B**, 259 (1985).
[34] F. Auger, B. Berthier, A. Cunsolo, A. Foti, W. Mittig, J. M. Pascaud, E. Plagnol, J. Québert, and J. P. Wieleczko, Phys. Rev. C **35**, 190 (1987).
[35] L. G. Sobotka, M. A. McMahan, R. J. McDonald, C. Signarbieux, G. J. Wozniak, M. L. Padgett, J. H. Gu, Z. H. Liu, Z. Q. Yao, and L. G. Moretto, Phys. Rev. Lett. **53**, 2004 (1984).
[36] R. J. Charity, M. A. McMahan, D. R. Bowman, Z. H. Liu, R. J. McDonald, G. J. Wozniak, L. G. Morreto, S. Bradley, W. L. Kehoe, A. C. Mignerey, and M. N. Namboodiri, Phys. Rev. Lett. **56**, 1354 (1986).
[37] R. J. Charity, D. R. Bowman, Z. H. Liu, R. J. McDonald, M. A. McMahan, G. J. Wozniak, L. G. Morreto, S. Bradley, W. L. Kehoe, and A. C. Mignerey, Nucl. Phys. **A476**, 516 (1988).
[38] R. J. Charity, M. A. McMahan, G. J. Wozniak, R. J. McDonald, L. G. Morreto, D. G. Sarantites, L. G. Sobotka, G. Guarino, A. Pantaleo, L. Fiore, A. Gobbi, and K. D. Hildenbrand, Nucl. Phys. **A483**, 371 (1988).
[39] D. R. Bowman, W. L. Kehoe, R. J. Charity, M. A. McMahan, A. Moroni, A. Bracco, S. Bradley, I. Iori, R. J. McDonald, A. C. Mignerey, L. G. Morreto, M. N. Namboodiri, and G. J. Wozniak, Phys. Lett. B **189**, 282 (1987).
[40] R. J. Charity, K. J. Jing, D. R. Bowman, M. A. McMahan, G. J. Wozniak, L. G. Morreto, N. Colonna, G. Guarino, A. Pantaleo, L. Fiore, A. Gobbi, and K. D. Hildenbrand, Nucl. Phys. **A511**, 59 (1990).
[41] H. Y. Han, K. X. Jing, E. Plagnol, D. R. Bowman, R. J. Charity, L. Vinet, G. J. Wozniak, and L. G. Moretto, Nucl. Phys. **A492**, 138 (1989).
[42] D. N. Delis, Y. Blumenfeld, D. R. Bowman, N. Colonna, K. Hanold, K. Jing, M. Justice, J. C. Meng, G. F. Peaslee, G. J. Wozniak, and L. G. Moretto, Z. Phys. A **339**, 279 (1991).
[43] D. N. Delis, Y. Blumenfeld, D. R. Bowman, N. Colonna, K. Hanold, K. Jing, M. Justice, J. C. Meng, G. F. Peaslee, G. J. Wozniak, and L. G. Moretto, Nucl. Phys. **A534**, 403 (1991).
[44] H. Ikezoe, N. Shikazono, Y. Tomita, Y. Sugiyama, K. Ideno, W. Yokota, Y. Nagame, S. M. Lee, M. Ogihara, S. C. Jeong, H. Fujiwara, and D. J. Hinde, Z. Phys. A **330**, 289 (1988).
[45] J. B. Moulton, J. E. Stephenson, R. P. Schmitt, and G. J. Wozniak, Nucl. Instrum. Methods **157**, 325 (1978).
[46] M. B. Tsang, D. Ardouin, C. K. Gelbke, W. G. Lynch, Z. R. Xu, B. B. Back, R. Betts, S. Saini, P. A. Baisden, and M. A. McMahan, Phys. Rev. C **28**, 747 (1983).
[47] R. Bass, Phys. Rev. Lett. **39**, 265 (1977).
[48] A. Gavron, Phys. Rev. C **21**, 230 (1980).
[49] A. J. Sierk, Phys. Rev. C **33**, 2039 (1986).
[50] J. R. Nix, Nucl. Phys. **A130**, 241 (1969).
[51] W. J. Swiatecki, Aust. J. Phys. **36**, 641 (1983).
[52] W. D. Myers and W. J. Swiatecki, Nucl. Phys. **81**, 1 (1966).
[53] J. Blocki, J. Randrup, W. J. Swiatecki, and C. F. Tsang, Ann. Phys. (N.Y.) **105**, 427 (1977).
[54] V. E. Viola, K. Kwiatkowski, and M. Walker, Phys. Rev. C **31**, 1550 (1985).
[55] V. E. Viola, Jr., Nucl. Data Tables A **1**, 391 (1966).
[56] F. Plasil, D. S. Burnett, H. C. Britt, and S. G. Thompson, Phys. Rev. **142**, 696 (1966).
[57] B. G. Glagola, B. B. Back, and R. R. Betts, Phys. Rev. C **29**, 486 (1984).
[58] L. G. Moretto and R. P. Scmitt, Phys. Rev. C **21**, 204 (1980).
[59] M. G. Itkis, R. Kalpakchieva, V. N. Okolovich, Yu. E. Penionzhkevich, and V. N. Tolstikov, Sov. J. Nucl. Phys. **36**, 483 (1982) [Yad. Fiz. **36**, 824 (1982)].
[60] M. E. Faber, Phys. Rev. C **24**, 1047 (1981).
[61] S. Cohen, F. Plasil, and W. J. Swiatecki, Ann. Phys. (N.Y.) **82**, 557 (1974).